8.4 ATOMIC-SCALE MECHANISMS OF HELIUM BUBBLE HARDENING IN IRON - Yuri N. Osetsky and Roger E. Stoller (Oak Ridge National Laboratory)

OBJECTIVE

The purpose of this research is to understand atomic level hardening mechanisms in materials with barriers such as voids, helium bubbles and rigid precipitates found in ODS alloys. This report covers effects of helium bubbles.

SUMMARY

Generation of helium in (n,α) transmutations changes the response of structural materials to neutron irradiation. The whole process of radiation damage evolution is affected by He accumulation and leads to significant changes in the material properties. A population of nanometer-size He-filled bubbles affects mechanical properties and the impact can be quite significant at high bubble density. Understanding how these basic mechanisms affect mechanical properties is necessary for predicting radiation effects. We completed an extensive study of the interactions between a moving edge dislocation and bubbles using atomic-scale modeling, focused on the effect of bubble size and He concentration in bubbles. The ability of bubbles to act as obstacles to dislocation motion is close to that of voids when the He-to-vacancy ratio is in the range 0 to 1. A few simulations at higher He contents demonstrated that the interaction mechanism is changed for over-pressurized bubbles and they become weaker obstacles. The results are discussed in light of post-irradiation materials testing.

Introduction

Generation of helium in materials under neutron irradiation occurs due to (n,α) transmutation reactions [1]. This phenomenon significantly changes the whole microstructure evolution for the commercially interesting temperatures above 600K and is a particular concern for future fusion applications due to elevated temperatures and high He-generation rates [2-3]. The need to develop predictive models for He effects has led to extended research programs worldwide (see e.g. [4].) According to the issues considered, studies of He effects can be generally considered in two categories.

One aspect is the prediction of He effects on microstructure evolution. This includes understanding the state of the He in the material and in bubbles, the interactions between mobile defects (vacancies, interstitial atoms) with He atoms and He-filled bubbles, and their impact within the appropriate models for microstructure evolution. There have been numerous studies of how helium generation influences cavity and other microstructural evolution using a range of simulation methods [5-8]. Recently we employed molecular dynamics simulations to study the behavior of He inside bubbles in an Fe matrix and its dependence on bubble size and temperature; this work led to the development of a modified equation of state for helium in bubbles [9]. In particular, it was found that the equilibrium He-to-vacancy (He/Vac) ratio obtained for bubbles 2 to 5 nm in diameter is about 0.4-0.7 at room temperature and weakly decreases with increasing temperature. This is quite consistent with recent experiments where the He/Vac ratio for small bubbles in ferritic-martensitic steels was determined using electron energy loss spectroscopy [10,11]. For example, helium density results for a 1.3 nm bubble lead to a He/vacancy ratio of 0.6 [10]. For bubbles from 2 to 5 nm, the He/vacancy ratio was in the range of 0.25–0.85 [11]. It is clear that He/Vac ratio depends on the irradiation temperature, rates of atomic displacements and He generation. However these numbers are an estimation of the He/Vac ratios to be considered.

The second aspect is the study of He as an impurity and in bubbles on mechanical properties. Although the first related modeling studies were reported quite a long time ago [12], this issue is much less explored for it demands quite a large-scale computing effort to receive robust results. The series of publications by Hafez Haghighat and Schaublin [13-16] is the most comprehensive research to date related to He bubble hardening in iron. The following conclusions can be formulated on the basis of results presented in [13-16]: 1) He-filled bubbles are strong obstacles consistent with corresponding size voids at He/Vac ≤ 2 and stronger than voids at He/Vac > 2; 2) bubble strength decreases at higher temperatures; and 3) there are certain quantitative but not qualitative effects on the bubble obstacle

strength at different He/Vac and temperatures when different Fe-matrix potentials [17-19] were used together with either the Wilson-Johnson [20] or Juslin-Nordlund [21] pair potentials for He-Fe interactions.

There are several aspects of this previous modeling work that should be mentioned. First, relatively small model crystals were used; as a result, the maximum dislocation length was 17 nm and the distance between dislocations in the periodic array was 25 nm even for large 7 nm diameter obstacles. Second, the quite high strain rate applied (the slowest reported is equal to $3x10^8$ s^{-1}) resulted in a dislocation velocity equal to 60 m/s. Third, very high He/Vac ratios of 1 to 5 were modeled. The mechanical stability of such bubbles was not investigated or reported.

Based on these observations, we conclude that many important aspects of dislocation interactions with helium bubbles require further attention to clarify the mechanisms involved. Among the most obvious issues are the following:

- Determining the obstacle strength of bubbles in the experimentally reasonable range of He content, i.e. He/Vac ratios ≤ 1,
- Understanding the sensitivity of the modeling results to the applied modeling parameters such as crystal size, strain rate and temperature,
- The atomic scale details of dislocation-bubble interaction mechanisms, and
- The stability and structure of over-pressurized bubbles with high He/Vac ratios and their temperature dependence.

Some of these issues were studied in the present research. However, we focus on one temperature, T=300K, because the majority of experimental mechanical testing has been performed at room temperature. We modeled bubbles with a relatively low He content, mainly He/Vac≤1, which is relevant to the experimental conditions. We report only a few cases with He/Vac=2 to demonstrate the dramatic change in the interaction mechanism due to over-pressurized conditions. Special attention was paid to the choice of modeling conditions and estimating the accuracy of the modeling results.

Atomic scale model

The atomic scale model we have used to study the ½<111> (110) edge dislocation interaction with He-filled bubbles is based on the molecular dynamics (MD) model described in [22]. This model describes a periodic array of dislocations and obstacles. The dislocation length, or equivalently, the distance between obstacles along the dislocation <112> line, is one of the most important modelling parameters. It should be long enough to permit the dislocation to adopt the necessary curvature at the critical state, i.e. before it is released from the obstacle. When interacting with strong obstacles, an edge dislocation usually adopts an "Orowan-like" configuration with an extended screw dislocation dipole formed in the obstacle's vicinity. This configuration may be called "Orowan-like" because it is similar to the dipole configuration that occurs for the true Orowan mechanism which involves impenetrable obstacles. It is important here that the interactions of screw segments belonging to the dipole are much stronger the interactions through the periodic boundaries along the dislocation line. In other words, the simulated dislocation segment length, L, should be much longer than the largest simulated obstacle diameter, D_O. In the present research we have used the constant L = 42 nm for the obstacle size up to D_O = 6 nm. Another important parameter is the crystal size along the $\boldsymbol{b}$ = ½<111> Burgers vector, $L_{\boldsymbol{b}}$. The importance of this parameter also arises because of the "Orowan-like" interaction mechanism; the length of the screw dislocation dipole at the critical state should be much smaller than $L_{\boldsymbol{b}}$ to minimize the contribution from the through-boundary interaction along the Burgers vector. In the present research the $L_{\boldsymbol{b}}$ value was chosen depending on the obstacle size and varied from ~30 nm to ~90 nm for obstacles from 1 nm to 6 nm in diameter. The crystal height, the measurement in the <110> normal direction to the dislocation slip plane, was chosen to be constant, H = 20 nm, for all the obstacles according to estimations described in [22]. The total number of lattice sites in the mobile crystals simulated was therefore varied from 2,074,024 to 6,236,064 depending on the obstacle size. The constant value of L allows direct comparison of the strength of all the obstacles. To generate force to move the dislocation, we have applied the strain rate loading described in [22]. We have used the constant strain rate value, $\dot{\varepsilon}$ = $5x10^6$ s^{-1}. The dislocation velocity depends on the applied strain rate and dislocation density and in the applied model can be estimated as: $v_D = \dot{\varepsilon}\, L_{\boldsymbol{b}} H / \boldsymbol{b}$ and varied from ~16 m/s to ~49 m/s in the smallest and largest crystals, respectively. The applied strain generates a

shear deformation of the modeled crystal which in turn generates shear stress (see [22] for how to calculate the shear stress value) which forces a dislocation to move. In MD modeling the instantaneous stress fluctuates depending on the temperature and dislocation velocity (i.e. applied strain rate.) Fig. 1 shows the variation of the instantaneous shear strain, τ, calculated every 100 time steps (the time step for motion equation integration is equal to 2fs) during the steady state motion of a ½<111>{110} edge dislocation under $5x10^6 s^{-1}$ applied strain rate modeled at 300K over 2.5 ns. One can see that its value fluctuates from <-20 MPa to almost 40 MPa. Statistical treatment resulted in the mean value $\bar{\tau}$=3.53 MPa (solid line in Fig. 1) and a standard deviation σ=9.8 MPa (the values of $(\bar{\tau} \pm \sigma)$ are indicated by point-dash lines in Fig. 1). Here we accepted the standard deviation as providing the most accurate estimate of the uncertainty in the mean shear stress. However, in the case of dislocation-obstacle interactions the uncertainty in the shear stress estimate should be higher because this process is far from the case of equilibrium steady state dislocation motion considered in Fig. 1. It is difficult to estimate this uncertainty for it depends on the temperature and applied strain rate. We cannot estimate the mean shear stress by a simple time average as in Fig. 1 for the interaction process is limited in time. More important is the obstacle release stress that exists over a limited and rather short time depending on the strain rate applied. As an example we illustrate the typical stress-strain, τ(ε), dependence obtained when modeling the interaction between a moving dislocation and a 2 nm bubble with He/Vac=0.5. The grey line presents the instantaneous shear stress calculated every 100 time steps. One can see that stress fluctuations are rather big and quite similar to that in Fig. 1 for the steady-state dislocation motion. To extract a reasonably averaged instantaneous value of τ we used adjacent average (AA) processing of the instantaneous data. The AA processing data with 5, 10 and 20 neighboring points (AA5, AA10 and AA20) are shown by green, black and red lines in Fig. 2. Data for AA20 show reasonably smooth behavior. We used this treatment to produce all of the results reported here, assuming as well that the uncertainty in estimating the shear stress values is the same as for the steady state dislocation motion at the same temperature where its lower limit is >10 MPa. Note that processing parameters (the number of neighboring points) and the shear stress uncertainty (standard deviation of the mean stress) depend upon the model strain rate and temperature; both values decrease at low temperature and $\dot{\varepsilon}$ and increase at higher temperatures and $\dot{\varepsilon}$. The maximum on the processed τ(ε) curve indicates the critical resolved shear stress (CRSS) which is the measure of the obstacle strength for a given interaction geometry. As shown in [22], if the dislocation segment, *L*, is long enough then CRSS ∝ 1/*L* for a given obstacle.

The atomic-scale interaction mechanisms were assessed using an on-the-fly visualization during simulation. For the dislocation line visualization we have used two techniques, either analyzing the common neighbors or the atomic disregistry in the dislocation core. The details can be found in [22].

To complete the description of the model accuracy, we consider one more issue related to the equilibration and annealing of simulated gas-filled bubbles: Any defect created in atomic-scale modeling requires a certain period of annealing to reach the equilibrium state. The He-filled bubble is an example that needs a long time to reach equilibrium depending on the size and He/Vac ratio as was reported recently in [9]. The need for a long equilibration time s demonstrated in [9], ~1-2 ns, to accurately estimate the value of He pressure inside small bubbles with low He/Vac ratios. For larger bubbles with higher He/Vac ratios, equilibration can be reached faster. The dynamics of temperature and pressure equilibration for He atoms inside a 4 nm bubble with He/Vac=0.4 is shown in Fig. 3. In this case the bubble reaches its equilibrium state sometime between 50 and 100 ps. In this study we annealed each crystal with the dislocation and bubble over this time before strain was applied.

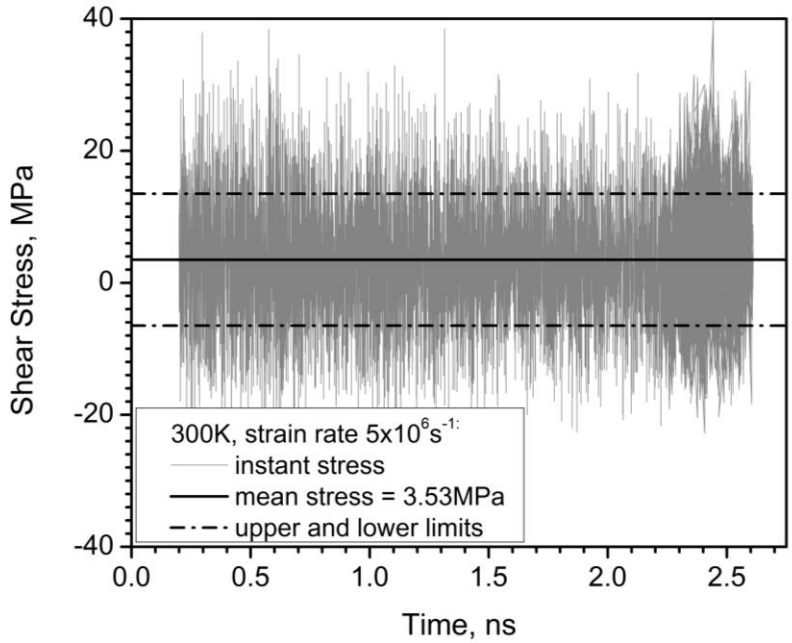

Figure 1. Modeling of steady state motion of ½<111>{110} dislocation at a strain rate of $5x10^6s^{-1}$ at 300K: grey line - instantaneous shear stress calculated every 100 time steps ; solid black line - mean value, 3.8MPa, estimated over 2.5ns, point-dash lines – mean stress plus/minus standard deviation value, σ = 9.8MPa.

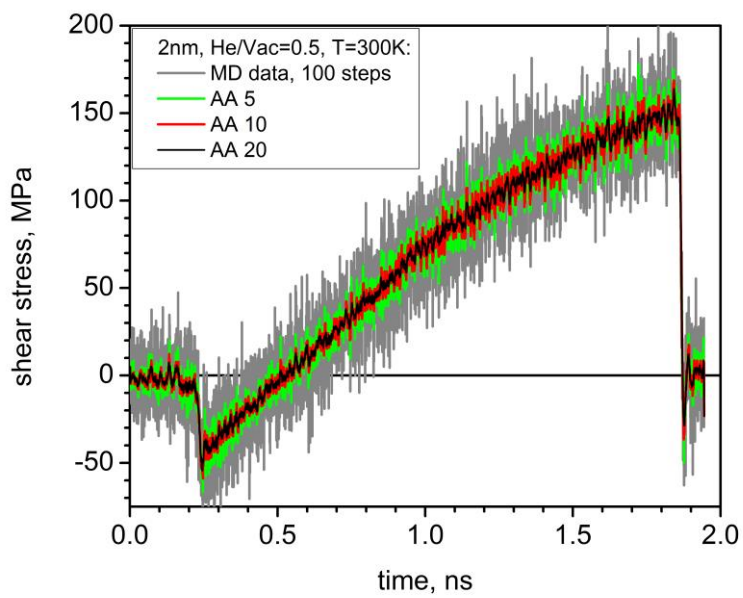

Figure 2. Stress-strain curve observed during dislocation interaction with 2 nm bubble with He/Vac=0.5: grey line - instantaneous shear stress calculated every 100 time steps; green, red and black lines – processes by adjacent average over 5, 10 and 20 neighbor points respectively.

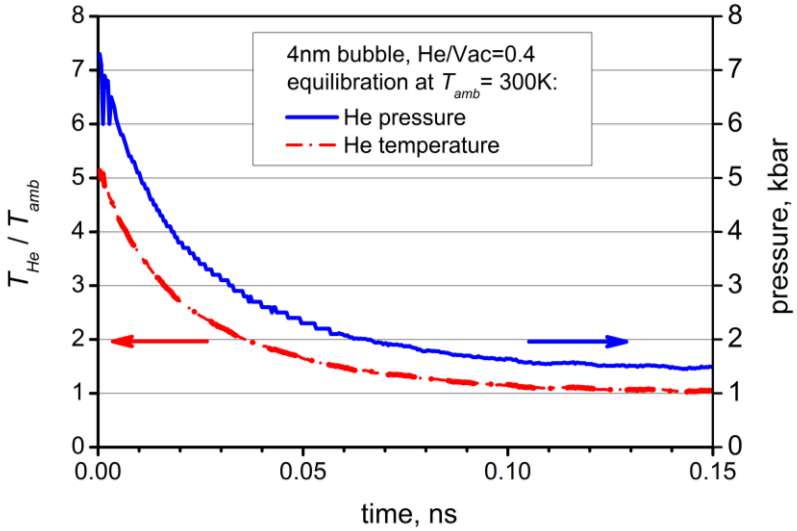

Figure 3. Evolution of He-atoms temperature and pressure inside the 4 nm bubble with He/Vac=1 during bubble equilibration.

For all simulations in this research we have used the following set of interatomic potentials: the embedded atom model potential for Fe from [17], the three-body potential for Fe-He interaction from [23, 24] and the pair potential for He-He interaction from [24]. The three-body He-Fe potential was fitted to a wide set of first principles data with the main emphasis on the properties of He-vacancy clusters [25]. This set of potentials was successfully applied in extensive studies of He-vacancy clusters, He-bubble nucleation, growth and stability and He transport in bcc Fe [9, 24, 25-28].

In this paper we report data for 1, 2, 4 and 6 nm diameter bubbles that contain up to 9640 vacancies and the corresponding number of He-atoms when the He/Vac ratio is varied from 0 to 1. The He/Vac ratio was extended up to 2 in the case of 2 nm bubbles to demonstrate when the interaction mechanism changes.

Results and discussion

The results for 1, 2, 4 and 6 nm bubbles are summarized in Fig. 4 which show the dependence of the CRSS on the He/Vac ratio. The size dependence is strong and follows that observed for voids. Moreover, within the presented values of He/Vac, the dislocation-bubble interaction mechanism is the same and very close to that of voids. To demonstrate this, we present a set of dislocation line configurations at some characteristic stages during its interaction with a 4 nm bubble with He/Vac=1 in Fig. 5. These states are fully compatible with similar states for the void described in [13]. In Fig. 5, State 1 is related to dislocation motion through the crystal before it comes into contact with the bubble. This is equivalent to the initial stage of $\tau(\varepsilon)$ curve shown in Fig. 2 when the shear stress is eventually constant. State 2 occurs when the dislocation is attracted by the bubble and comes into contact. This state is characterized by a strong attractive force and is accompanied with the sudden drop of shear stress to the negative value in Fig. 2. When dislocation intersects the bubble it loses a certain amount of dislocation line length. This is energetically favorable for the dislocation line energy inside the bubble can be set to 0 (a similar effect is demonstrated for a void in [13].) At State 3, the dislocation crosses the bubble along its diameter and therefore loses the longest possible segment. This is the minimum energy and a zero stress state. It is equivalent to the point when $\tau(\varepsilon)$ curve intersects zero stress level at about ε=0.25 in Fig. 2. Further straining leads to dislocation glide over the bubble surface, restoring the dislocation line in the crystal and creating a step on the exit surface of the bubble. During this process the shear stress increases and dislocation line curve due to glide of the segments in the crystal. State 4 in Fig. 5 shows the critical shape of the dislocation just before it breaks out. The considered obstacle is “strong” and the initial edge dislocation creates a relatively long dipole of screw segments with a near-zero angle between them. As mentioned above, the dislocation is similar to that obtained by the Orowan mechanism for impenetrable

obstacles. The only difference between this and the true Orowan mechanism is the distance between dipole segments. In the case of impenetrable obstacles, this is equal to the obstacle diameter in the dislocation slip plane. In the case of bubbles and voids, this can be much shorter due to the dislocation glide over the bubble surface and the screw segments cross-slip. The State 4 in Fig. 5 is characterized by the maximum value on the τ(ε) curve. Finally, State 5 occurs when the dislocation is released from the bubble and glides through the crystal.

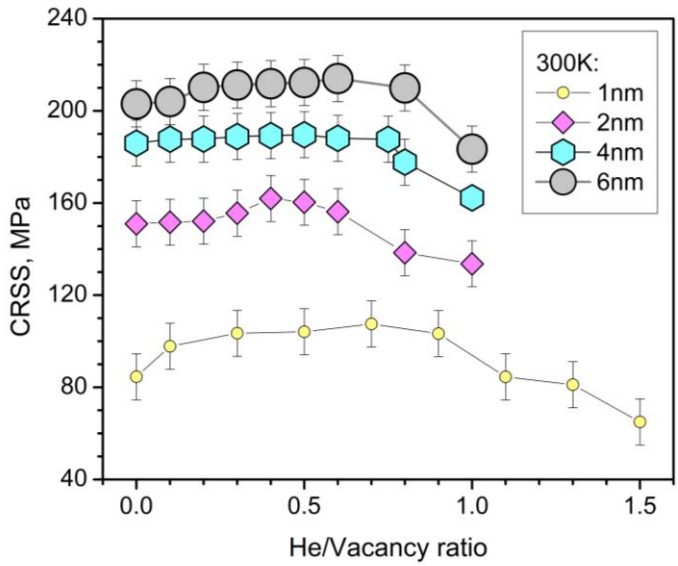

Figure 4. Dependence of the critical resolved shear stress versus He/Vac ratio for bubbles of 1, 2, 4 and 6 nm in diameter

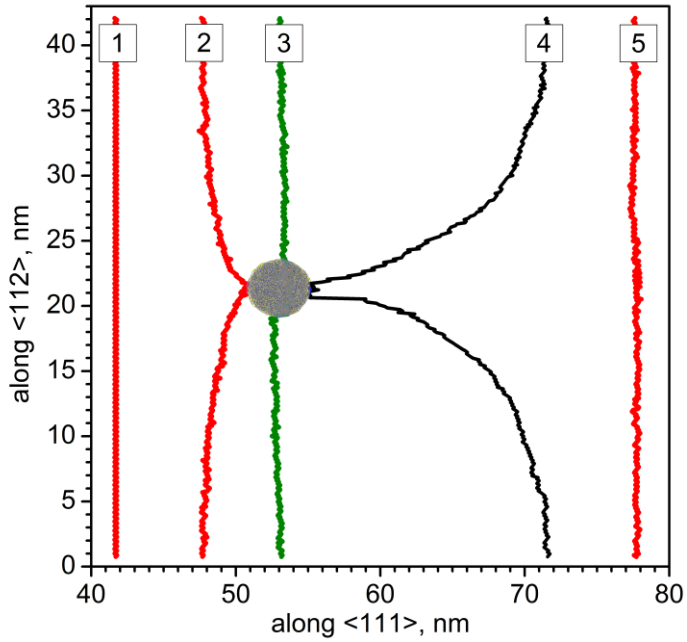

Figure 5. Shape of the dislocation line in the {110} slip at different stages during interaction with 4 nm bubble with He/Vac=1. Stages 1 to 5 are explained in the text.

The mechanism described above was observed for all the bubbles with He/Vac≤1. According to Fig. 5, and considering the uncertainty in the CRSS value definition of >10 MPa, the dependence of CRSS is rather weak for He/Vac≲0.8. However, we observed some differences between the interactions with low- and high- He content bubbles. One example of these differences is demonstrated in Fig. 6 which shows the dislocation line shape after it is released from a 4 nm bubble with different He/Vac. At He/Vac=0, i.e. a void, the line eventually climbs up absorbing vacancies from the obstacle. Visualization of this interaction has shown that one of the two screw segments that terminate at the void surface (see i.e. State 4 in Fig. 5) cross-slips up creating the corresponding superjog after the dipole is released from the void. A similar mechanism for other voids in Fe was discussed in [29]. However, a monotonic increase in He/Vac ratio, reduces the number of absorbed vacancies, and at He/Vac=1, the dislocation line absorbs more atoms and climbs down (see the corresponding dislocation line in Fig. 6). In this case one of the two screw dislocation segments climb down declines rather than up at lower He/Vac values.

As was pointed out in [30] such climb reduces the CRSS; however, the mechanism is not yet understood. The data obtained here, e.g. the CRSS (Fig. 4) and dislocation line shapes (Fig. 6) are in principle consistent with the maximum CRSS values usually being correlated with the minimum climb (and therefore the weakest cross-slip). However, this conclusion should be verified on other examples because of the high uncertainty in CRSS values. The only confident conclusion we can make is that at the highest He content studied here, He/Vac=1, all the bubbles are weaker than the corresponding voids.

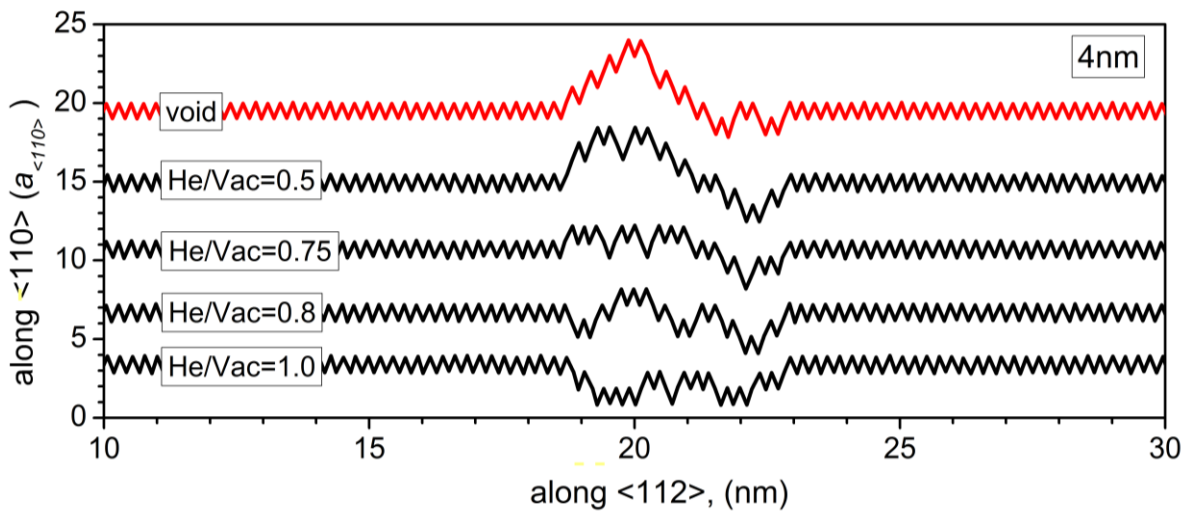

Figure 6. Shape of the dislocation line viewed along the Burgers vector after interaction with 4 nm bubbles with different He/Vac ratios.

To explore the effect of high He concentration, we modeled a 2 nm bubble with He/Vac=2. The τ(ε) curves for some He/Vac values are presented in Fig. 7 and the corresponding dislocation line shapes in Fig. 8. Obvious qualitative differences are observed in the both figures. In Fig. 7 the τ(ε) curve for He/Vac=2 is completely different from all the others with He/Vac≤1. The corresponding line shape demonstrates a significant amount of climb down that is equivalent to 36 atoms absorbed by the line. This means that the 2 nm bubble, that occupies 339 vacancy sites, increased its volume by more than 10%. Visualization of the interaction mechanisms has confirmed that it is qualitatively different from all other cases considered so far. During the equilibration process the bubble shape changed from the high symmetric sphere to some irregular shape that expanded locally. This occurred because for He/Vac=2 at T=300K the bubble is strongly over-pressurized and the bubble surface is deformed significantly outwards toward the Fe matrix but no clear punching of interstitial atoms was observed at this stage. However, when the dislocation approached the bubble it “emitted” an interstitial cluster that attracted the dislocation. This can be seen as a sudden drop on the corresponding τ(ε) curve on Fig. 7. The cluster was absorbed by the line creating a superjog and the dislocation was repelled from the bubble. At this state the

corresponding τ(ε) curve on Fig. 7 abruptly increased. At the next stage, due to continuous straining the jogged dislocation was pushed towards the bubble. However, unlike the other cases when the straight dislocation line intersected the bubble in the equatorial plane, the heavily jogged line just touches the periphery of the deformed bubble. As a result, the dislocation line now does not shear the whole bubble and the CRSS decreases by almost 40%. It is obvious that the over-pressurized bubble state arising from such a high He/Vac ratio is responsible for this change in the interaction mechanism.

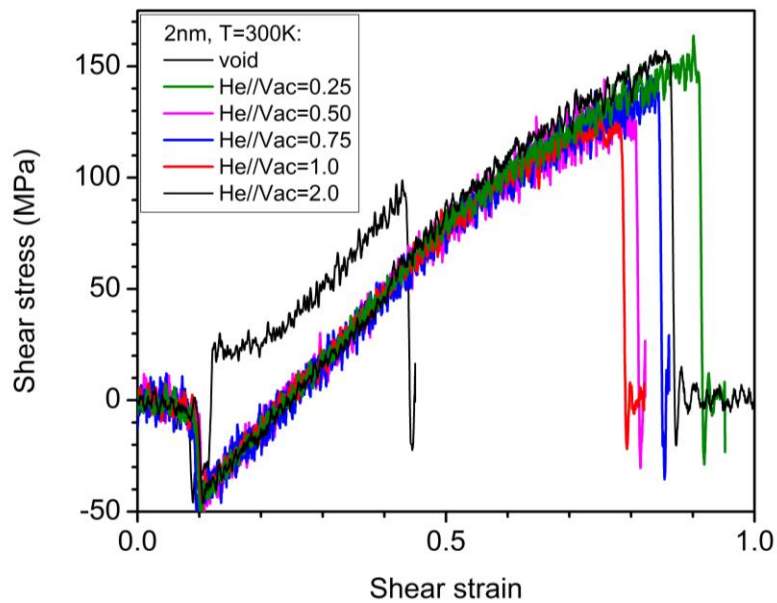

Figure 7. Stress-strain curves obtained during dislocation interaction with 2 nm bubbles with different He/Vac ratios.

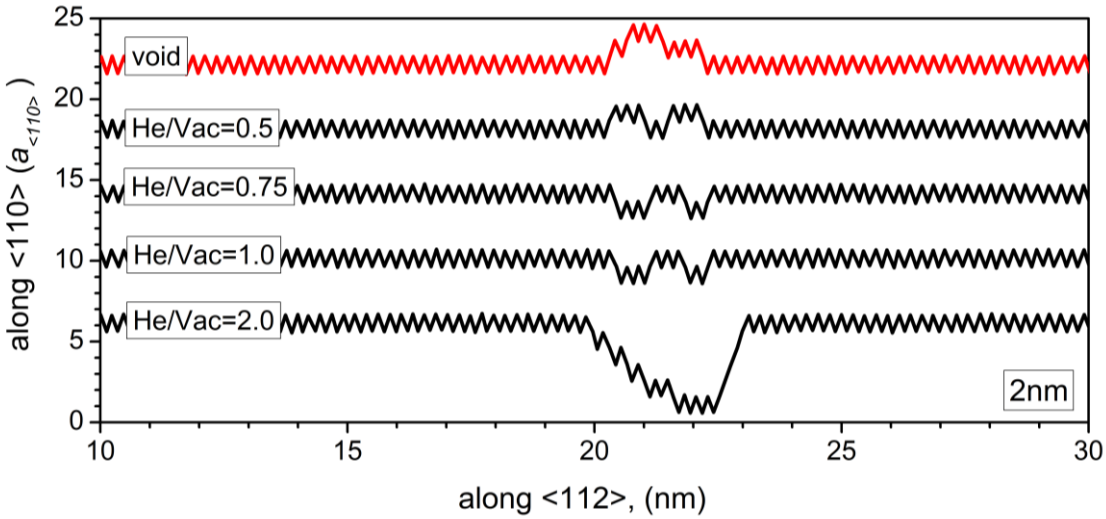

Figure 8. Shape of the dislocation line viewed along the Burgers vector after interaction with 2 nm bubbles with different He/Vac ratios.

We should note that CRSS decrease at He/Vac ≃ 2 as was reported earlier in [15-17]; however, the detailed mechanism and the difference with lower He-content bubbles was not described. Here we

confirm the drop in CRSS and identify the mechanism for the case of 2 nm bubble with He/Vac=2 at T=300K. We expect a similar decrease in CRSS for other sizes, which should be temperature dependent. The higher He-content bubbles studied in [15-17] demonstrated a significant increase in CRSS for up He/Vac=2-5, however the interacting mechanisms were not described. We expect that at such a high He-content a bubble should punch out interstitial clusters well before the dislocation approaches it, and in this case the interaction mechanism could be quite different than we observed with He/Vac=2. The difference is that in the present case the interstitial cluster was released from the bubble due to the strain fields from the approaching dislocation. It was released, a) in the place and b) with the orientation corresponding to the minimum interaction energy. These are, a) the negative pressure volume below the dislocation slip plane, and b) interstitial atom orientation along the dislocation Burgers vector. This correlated formation of an interstitial cluster from the over-pressurized bubble is the mechanism that reduces CRSS for a given size within a certain He/Vac and temperature range. However, if the He/Vac is much higher a strongly over-pressurized bubble may punch single interstitials or interstitial clusters out during its equilibration independent of the dislocation. In these cases interstitial clusters should be much larger (due to a much higher pressure) and their position and direction do not correlate with the dislocation stress fields. Therefore, dislocation-bubble interaction mechanism may be different for it may now involve interaction with the separate large interstitial cluster at the same time. The key issue here is the behavior of strongly over-pressurized bubbles and how the He/Vac ratio, temperature and bubble size affect the interstitial cluster punching, i.e. cluster size, formation geometry and crystallography. Once these mechanisms are understood their effect on dislocation-bubble interactions can be rationalized using a computational approach similar to that applied here. This work is now in progress.

We should also note that the size scale of dislocation-bubble interaction mechanisms is, in principle, compatible with direct transmission electron microscopy *in situ* straining experiments. It may be possible to study different mechanisms by performing *in situ* straining at different temperatures and therefore change the bubble pressure. Large scale atomistic simulations could then reproduce experimental conditions (except for the strain rate) to help in understanding the mechanisms observed. A similar direct modeling experiment comparison was made in previous studies of dislocation interactions with stacking fault tetrahedra when new mechanisms were discovered [30].

Summary

A large-scale atomistic study using molecular dynamics simulations was carried out to investigate the detailed interactions of moving edge dislocations with helium bubbles in iron. The important physical parameters of the computational model and their effects on the accuracy and uncertainty of simulation results were studied. Some of these issues are general, such as the accuracy of the shear stress definition, while others are specific to the behavior of gas-filled bubbles, such as the required equilibration time. The study focused on the interaction between a moving ½<111>{110} edge dislocation, and bubbles in the size range of 1 to 6 nm diameter, with the physically-relevant but so-far unexplored range of He-to-vacancy ratio from 0 to 1 at a temperature of 300K. The primary results include:

1. These bubbles demonstrate qualitatively the same hardening mechanism as that obtained earlier for voids,
2. The strength of these bubbles was found to be weakly dependent on. He/Vac ratio within the range of 0 to ~0.8. At higher He/Vac ratios the bubble strength decreases.
3. The over-pressurized 2 nm bubble with He/Vac=2 has demonstrated a completely different strengthening mechanism which i about 40% weaker. In this mechanism the over-pressurized bubble emits an interstitial cluster under the influence of the approaching dislocation strain fields. Correlated emission of interstitial clusters minimizes the dislocation-bubble intersection and the maximum shear stress.
4. The results are compared with those available in the literature and the possible mechanisms for strongly over-pressurized bubbles are discussed.

References.

[1] R. E. Stoller, Journal of Nuclear Materials 174 (1990) 289-310..

[2] H. Schroeder, P. Batfalsky, *J. Nucl. Mater.* 117 (1983) 287.
[3] T. Yamamoto, G.R. Odette, P. Miao, D.T. Hoelzer, J. Bentley, N. Hashimoto, H. Tanigawa, and R.J. Kurtz, *J. Nucl. Mater.* 367-370 (2007) 399-410.
[4] B.D. Wirth, G.R. Odette, J. Marian, L. Ventelon, J.A. Young-Vandersall, L.A. Zepeda-Ruiz, *J. Nucl. Mater.* **103** (2004) 329.
[5] N. M. Ghoniem, J. Nucl. Mater. 174 (1990) 168-177.
[6] R. E. Stoller and G. R. Odette, "The Effect of Helium on Swelling: Influence of Cavity Density and Morphology," Effects of Radiation on Materials, ASTM STP 782, H. R. Brager and J. S. Perrin, Eds., American Society of Testing and Materials, Philadelphia, 1982, pp. 275-294.
[7] J. B. Adams and W. G. Wolfer, J. Nucl. Mater. 166 (1989) 235-242.
[8] A. Caro, J. Hetherly, A. Stukowski, M. Caro, E. Martinez, S. Srivilliputhur, L. Zepeda-Ruiz, M. Nastasi, J. Nucl. Mater. 418 (2011) 261-268.
[9] R.E.Stoller and Y.N.Osetsky, *J. of Nucl. Mat.* **455** (2014) 258–262.
[10] Y. Wu, G.R. Odette, T. Yamamoto, J. Ciston, P. Hosemann, "An Electron Energy Loss Spectroscopy Study of Helium Bubbles in Nanostructured Ferritic Alloys," Fusion Reactor Materials, Semiannual Progress Report DOE/ER-0313/54, Oak Ridge National Laboratory (2013) 173–179.
[11] S. Fréchard, M. Walls, M. Kociak, J.P. Chevalier, J. Henry, D. Gorse, *J. Nucl. Mater.* **393** (2009) 102.
[12] M.I. Baskes, M.S.Daw, "The Effects of Impurities on Dislocation Dynamics and Fracture: An Atomistic Study", 4th International Conference on Hydrogen Effects on Material Behavior (Jackson Lake Lodge, WY: 1989), Published: Tms (September 1989), ISBN-10: 0873391500.
[13] R. Schaublin and Y.L. Chiu, *J. Nucl. Mater.* **362** (2007) 152.
[14] S S.M. Hafez Haghighat and R. Schaeublin, "Molecular dynamics modeling of cavity strengthening in irradiated iron", Proceedings of Third International Conference of Multiscale Materials Modeling, Freiburg, Germany, September 2006, p.729.
[15] S.M. Hafez Haghighat and R. Schaeublin, *J. Comput. Aided Mater. Des.* **14** (2008) 191.
[16] S.M. Hafez Haghighat and R. Schaublin, *Philos. Mag.* **90** (2010) 1075.
[17] G.J. Ackland, D.J. Bacon, A.F. Calder and T. Harry, *Phil. Mag.* A **75** (1997) 713.
[18] M.I. Mendelev, S. Han, D.J. Srolovitz, D.Y. Sun and M. Asta, *Phil. Mag.* **83** (2003) 3977.
[19] S.L. Dudarev and P.M. Derlet, J. Phys. *Condens. Matter.* **17** (2005) 7097.
[20] W.D. Wilson and R.A. Johnson, in Rare Gases in Metals, P.C. Gehlen, J.J. Beeler and R.J. Jaffe, eds., Premium Press, NY, 1972, 375.
[21] N. Juslin and K. Nordlund, *J.Nucl.Mater.* **382** (2008) 143.
[22] Yu.N. Osetsky and B.J. Bacon, Model. *Simul., Mater. Sci. and Eng.* **11** (2003) 427.
[23] T. Seletskaia, Yu.N. Osetskiy, R.E. Stoller and G.M. Stocks, *J. Nucl. Mater.* **361** (2007) 52-61.
[24] R.E. Stoller, S.I. Golubov, P.J. Kamenski, T. Seletskaia, Yu.N. Osetsky, *Philos. Mag.* **90** (2010) 923.
[25] R.A. Aziz, A.R. Janzen and M.R. Moldovan, *Phys. Rev. Let.* **74** (1995) 1586.
[26] T. Seletskaia, Yu.N. Osetsky, R.E. Stoller and G.M. Stocks, *J. Nucl. Mater.* **351** (2006) 109-118.
[27] D.M. Stewart, Yu. N. Osetskiy, R.E. Stoller, *J. Nucl. Mater.* **417** (2011) 1110.
[28] D.M. Stewart, Yu.N. Osetsky, R.E. Stoller, S. I. Golubov, T. Seletskaia, P.J. Kamenski, *Philos. Mag*. **90** (2010) 923.
[29] Yu.N. Osetsky and D.J. Bacon, *Philos. Mag*. **90** (2010) 945.
[30] Yu.N. Osetsky, Y. Matsukawa, R.E. Stoller and S.J. Zinkle, *Philos. Mag. Lett.* **86** (2006) 511.